S-layer is a key element in metabolic response and entry into the stationary phase in Bacillus cereus AH187

Cécile Boutonnet, Christian Ginies, Béatrice Alpha-Bazin, Jean Armengaud, Alice Château, Catherine Duport

Journal of Proteomics 289 (2023) 105007

Contents lists available at ScienceDirect

Journal of Proteomics

journal homepage: www.elsevier.com/locate/jprot

S-layer is a key element in metabolic response and entry into the stationary phase in *Bacillus cereus* AH187

Cécile Boutonnet [a], Christian Ginies [a], Béatrice Alpha-Bazin [b], Jean Armengaud [b], Alice Château [a], Catherine Duport [a,*]

[a] Avignon Université, INRAE, UMR SQPOV, F-84914 Avignon, France
[b] Université Paris Saclay, CEA, INRAE, Département Médicaments et Technologies pour la Santé (DMTS), SPI, 30200 Bagnols-sur-Cèze, France

ARTICLE INFO

Keywords:
S-layer
Bacillus cereus
Proteome reallocation
Stationary-phase stress response

ABSTRACT

Bacillus cereus is a food-borne Gram-positive pathogen. The emetic reference strain *B. cereus* AH187 is surrounded by a proteinaceous surface layer (S-layer) that contributes to its physico-chemical surface properties, and promotes its adhesion in response to starvation conditions. The S-layer produced by *B. cereus* AH187 is composed of two proteins, SL2 and EA1, which are incorporated at different growth stages. Here, we showed that deletion of the genes encoding SL2 and EA1 produced viable cells, but decreased the glucose uptake rate at the start of growth, and induced extensive reorganization of the cellular and exoproteomes upon entry into the stationary phase. As a consequence, stationary cells were less resistant to abiotic stress. Taken together, our data indicate that the S-layer is crucial but comes at a metabolic cost that modulates the stationary phase response.

Significance: The emetic strains of *Bacillus cereus* are known to cause severe food poisoning, making it crucial to understand the factors contributing to their selective enrichment in foods. Most emetic strains are surrounded by a crystalline S-layer, which is a costly protein structure to produce. In this study, we used high-throughput proteomics to investigate how S-layer synthesis affects the allocation of cellular resources in the emetic *B. cereus* strain AH187. Our results demonstrate that the synthesis of the S-layer plays a crucial role in the pathogen's ability to thrive under stationary growth phase conditions by modulating the stress response, thereby promoting its lifestyle as an emetic pathogen. We conclude that the synthesis of the S-layer is a critical adaptation for emetic *B. cereus* to successfully colonize specific niches.

1. Introduction

Bacillus cereus is a food-borne Gram-positive pathogen that causes two distinct illness syndromes: diarrhea and emesis [1]. Emesis is attributed to the toxin cereulide, a heat- and acid-stable cyclic dodecadepsipeptide, which is produced in food matrices by emetic *B. cereus* strains. Emetic strains differ from other *B. cereus* strains in terms of natural primary habitat (roots and tubers) and by their prevalence in food [2]. In addition, they form a distinct cluster within the *B. cereus* group, with specific growth, resistance, and morphological characteristics. One morphological specificity of emetic *B. cereus* strains is the presence of an S-layer at their cell surface, as reported for the emetic reference strain *B. cereus* AH187 (also named F4810/72) [3].

Bacterial S-layers are composed of one or more (glyco)proteins – S-layer proteins (SLPs) – that self-assemble to form a contiguous paracrystalline array covering the entire cell surface. Assembly of the S-layer requires high protein flux across the cell envelope that depends on the accessory Sec secretion system in Gram-positive bacteria [4]. In Gram-positive bacteria, the S-layer is anchored to the cell surface via non-covalent interactions with cell wall polysaccharides [5–7]. The S-layer of *B. cereus* AH187 is composed of two SLPs, SL2 and EA1. The proportion of these two proteins at the cell surface depends on both the growth medium and the physiological status of the *B. cereus* cells. Lack of SL2 and EA1 synthesis modifies the physicochemical properties of exponentially grown *B. cereus* cells and decreases the hydrophobic properties of stationary phase *B. cereus* cells, altering their capacity to adhere to abiotic surfaces under non-stressful growth conditions [3].

S-layer assembly represents a significant metabolic burden for the microorganism due to the high abundance of SLPs and the need to export them from the cytoplasm to the cell surface [8,9]. In stressful growth conditions, such as those encountered in oligotrophic medium or at low temperature, *B. cereus* AH187 loses its capacity to produce the S-layer, or

* Corresponding author.
E-mail address: catherine.duport@univ-avignon.fr (C. Duport).

https://doi.org/10.1016/j.jprot.2023.105007
Received 7 April 2023; Received in revised form 21 August 2023; Accepted 14 September 2023
Available online 18 September 2023

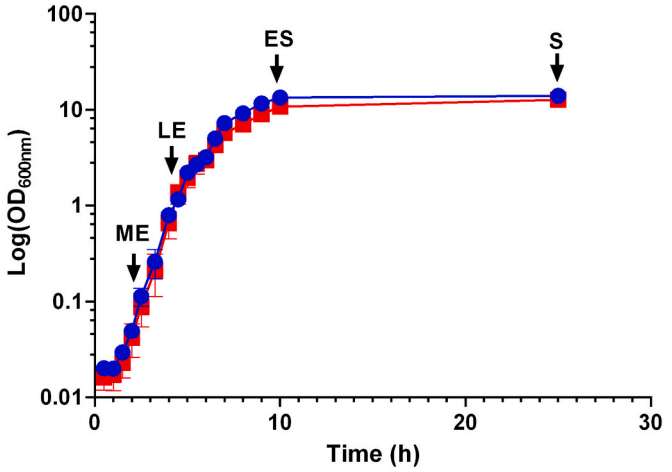

Fig. 1. Growth curves for WT and Δ*sl2*Δ*eag* strains. Cells were grown at 37 °C in MODG medium. Samples for proteomics analysis were collected at mid-exponential (ME), late exponential (LE), early stationary (ES), and stationary (S) growth phases, as indicated. The blue colour represents the WT strain and the red colour represents the Δ*sl2*Δ*eag* strain. (For interpretation of the references to colour in this figure legend, the reader is referred to the web version of this article.)

synthesizes lower quantities of SL2, probably to re-allocate resources and energy to mechanisms improving resilience [10,11]. Under non-stressful growth conditions, no growth deficit is associated with S-layer production [3], suggesting that *B. cereus* cells circumvent the metabolic burden of producing an S-layer by compensatory metabolic adaptations [12]. However, this assumption remains to be proven, and the physiological and cellular consequences of such adaptation need to be investigated.

In this study, we compared the dynamics of the whole-cell proteome and the exoproteome of the S-layer deficient strain *Δsl2Δeag* and its parent *B. cereus* AH187 during growth in defined MODG medium [13]. By examining both the whole-cell proteome and the exoproteome, we gained a comprehensive understanding of the bacterium's responses, as these two proteomic components offer distinct yet complementary insights [14]. The data showed that S-layer production in *B. cereus* AH187 cells increased the rate of glucose uptake at the beginning of growth, and was accompanied by reorganization of the stationary phase regulatory network. As a result, S-layer-producing bacteria were more resistant to salt and cold stress, suggesting that the S-layer increases the fitness of emetic strains to deal with challenging environmental conditions.

2. Material and methods

2.1. Bacterial strains, growth conditions, and sample preparation

The wild-type (WT) *B. cereus* AH187 (or F4810/72) was originally isolated from vomit [15]. It was used alongside its Δ*sl2*Δ*eag* deletion mutant, lacking the S-layer [16]. Strains were grown at 37 °C with shaking (200 rpm) in MOD medium supplemented with 30 mM glucose (MODG) and buffered at pH 7.2 [22]. Cultures were inoculated in MODG medium (500 mL in 2-L pre-heated Erlenmeyer flasks) at an OD_{600nm} of 0.02 (i.e. 3×10^6 CFU/mL) from overnight precultures. Samples of each culture were collected by centrifugation (10 min, 10,000 g, at 4 °C) at mid-exponential (ME), late exponential (LE), early stationary (ES), and stationary (S) growth phases, as indicated in Fig. 1. Pellets – whole cells – and 0.2-μm filtered supernatant – exoproteome – were analyzed by proteomics. Glucose, amino acids, and proteases were also quantified in filtered supernatant samples.

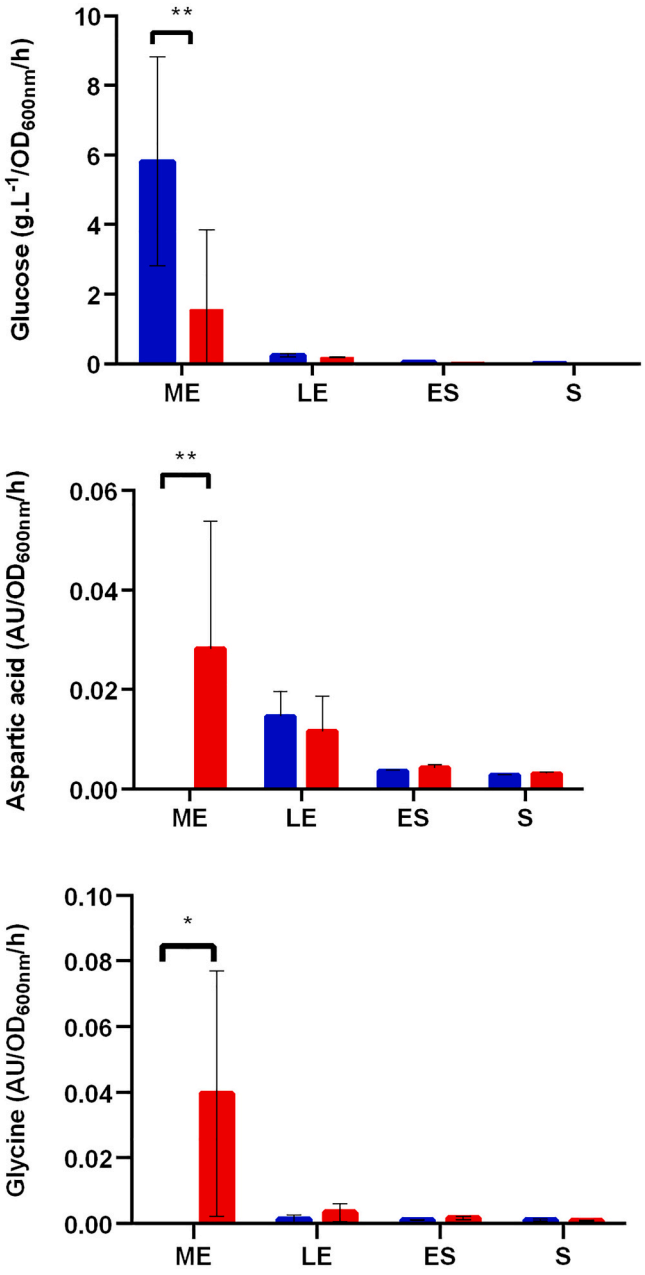

Fig. 2. Growth-related parameters of Δ*sl2*Δ*eag* and WT strains. Specific consumption of glucose, aspartic acid, and glycine by WT (blue) and Δ*sl2*Δ*eag* (red) cells at mid-exponential (ME), late exponential (LE), early stationary (ES), and stationary (S) growth phases. *, $p < 0.1$; **, $p < 0.01$. (For interpretation of the references to colour in this figure legend, the reader is referred to the web version of this article.)

2.2. Protein identification by nano-liquid chromatography-coupled with tandem mass spectrometry (nanoLC-MS/MS) and label-free quantification

Protein extracts were prepared from cell pellets and culture supernatants as previously described [17]. Proteins from WT and *Δsl2Δeag* culture supernatants were TCA-precipitated, and the resulting pellets were dissolved in NuPAGE buffer. Protein samples were loaded onto NuPAGE Bis-Tris 4–12% gels (Invitrogen) for a short 5-min migration at 200 V [18]. Proteins were digested *in gel* with sequencing-grade ProteaseMAX trypsin (Promega) according to the supplier's protocol. Triplicate samples were prepared for the two strains – WT and *Δsl2Δeag* mutant. Peptide mixtures were analyzed by nanoLC-MS/MS using an Ultimate 3000 nano LC system coupled to a Q-Exactive HF mass

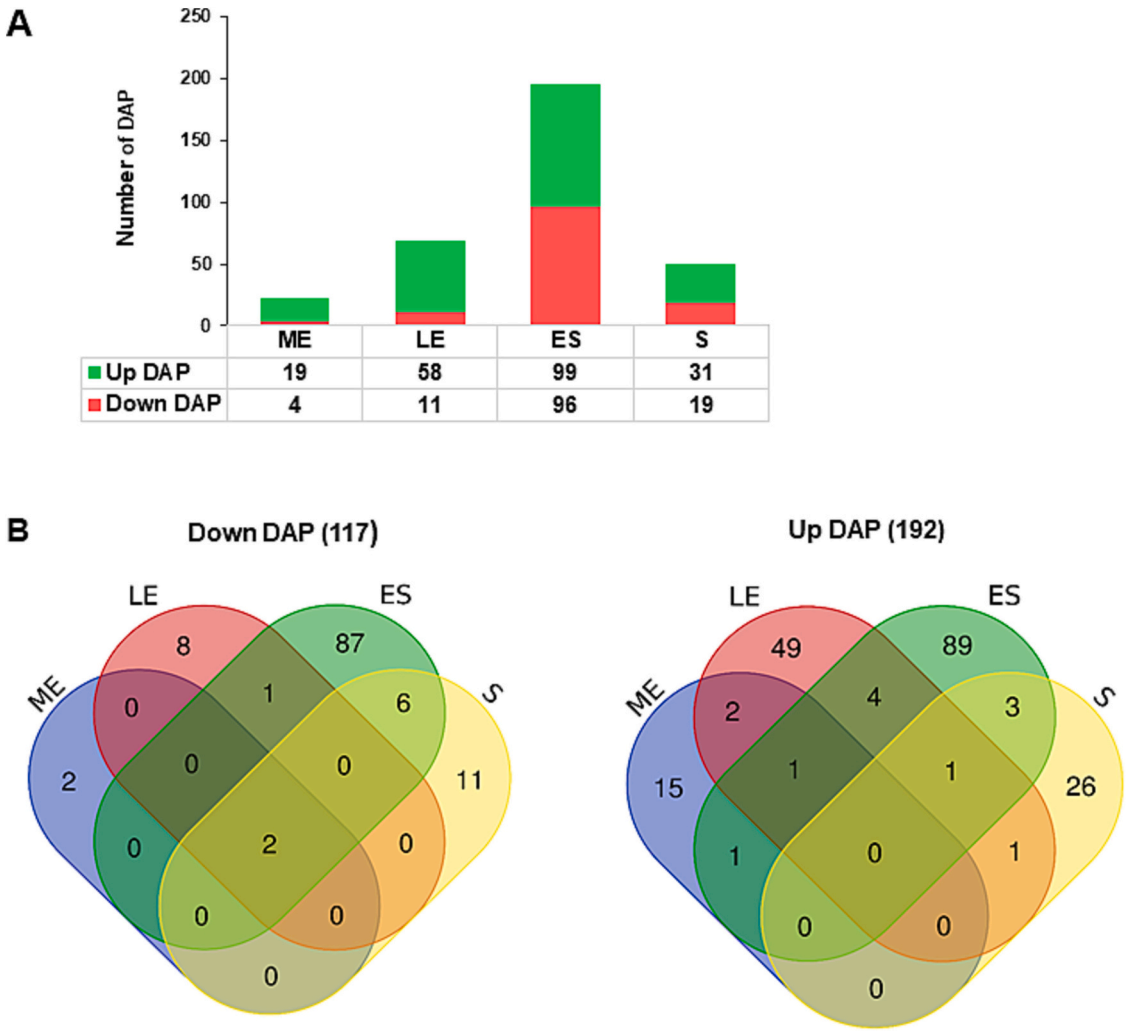

Fig. 3. Dynamics of cellular proteins differentially accumulating (DAPs) in the *Δsl2Δeag* mutant compared to WT. A. Bar charts showing up- and down-DAPs at mid-exponential (ME), late exponential (LE), early stationary (ES), and stationary (S) growth phases. The numbers of up-DAPs (green) and down-DAPs (red) are shown above each bar. B. Venn diagrams of down- and up-DAPs identified at the different time-points. The number of specific and overlapping DAPs are given. (For interpretation of the references to colour in this figure legend, the reader is referred to the web version of this article.)

spectrometer (Thermo Fisher Scientific, Illkirch-Graffenstaden, France), as previously described [11]. Briefly, after loading, peptides were desalted online on a reverse-phase Acclaim PepMap 100 C18 precolumn (100-Å pore size, 300 µm i.d. × 5 mm), and then resolved on a nanoscale Acclaim Pepmap 100 C18 column (3-µm bead size, 100-Å pore size, 75 µm id x 500 mm) at a flow rate of 200 nL.min^{-1}. Solvent A (0.1% formic acid) and solvent B (0.1% formic acid and 80% CH_3CN) were used to form the gradient for peptide separation. For cellular proteins, a 90-min gradient (from 4% to 25% B in 75 min followed by an increase to 40% B) was used. For extracellular proteins, a 60-min gradient (from 2.5% to 25% B in 50 min followed by an increase to 40% B) was applied. Tryptic MS/MS spectra were matched against the *B. cereus* AH187 NCBI_20,200,622 database using the MASCOT Daemon search engine. Parameters included a mass tolerance of 5 ppm for the parent ion and 0.02 Da for the MS/MS fragments, 2^+ or 3^+ peptide charge, a maximum of two missed cleavages, cysteine carbamidomethylation as fixed modification, and methionine oxidation as variable modification. Peptide-to-Spectrum Matches with a *p*-value ≤0.05 in homology threshold mode were retained. Protein identification was validated by at least two distinct peptides upon parsing with IRMa software v1.3.1 [19], resulting in a false discovery rate lower than 1%. Normalized spectral abundance factor (NSAF) values were calculated by dividing the number of spectra assigned to a protein in a given sample by its molecular weight [20]. Protein abundance was compared between WT and *Δsl2Δeag* mutant by applying the TFold test [21]. Proteins were considered differentially accumulated when $p < 0.05$ and fold-change ≥1.5. All mass spectrometry proteomics data have been submitted to the ProteomeXchange Consortium via the PRIDE partner repository under dataset identifiers PXD040271 and https://doi.org/10.6019/PXD040271.

2.3. Methylchloroformate (MCF) derivatization and Gaz chromatography mass spectrophotometry (GC–MS) analysis

Analytical analysis was performed by the methylchloroformate (MCF)-based alkylation derivatization technique [22]. Filtered supernatant (60 µL) was resuspended in 100 µL of 2 M NaOH in a hemolysis tube. Methanol (167 µL) and pyridine (34 µL) were added to the suspension. MCF (20 µL) was added, and the mixture was vigorously vortexed for 30 s. This step was repeated once. To remove excess reagent and extract the derivative compound, 400 µL chloroform was added, and the mixture was vortexed for 10 s, then 400 µL 50 mM $NaHCO_3$ was added, and the mixture was vortexed for 10 s once again. The organic phase was collected for GC–MS analysis. An alanine d_4 sample at 1.58 mg.mL^{-1} was derivatized as a control (Cambridge Isotope Laboratories, Inc.). Derivatized samples were analyzed by capillary column gas chromatography (ZB-5MS 30 m, 0.25 mm i.d., 0.5 µm film thickness,

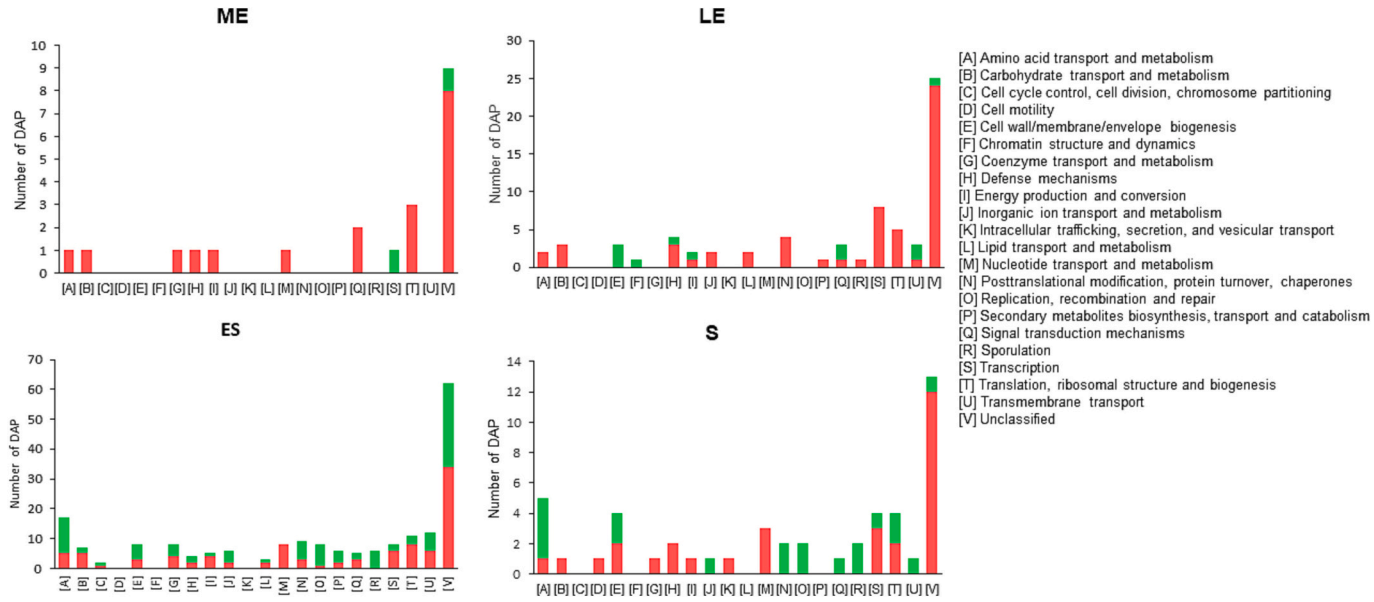

Fig. 4. Clusters of orthologous groups (COG) distribution of cellular proteins differentially accumulating (DAPs) in the Δ*sl2*Δ*eag* mutant compared to WT. DAPs were clustered at mid-exponential (ME), late exponential (LE), early stationary (ES), and stationary (S) growth phases. The number of up-DAPs is indicated in green and down-DAPs in red, in each COG group. (For interpretation of the references to colour in this figure legend, the reader is referred to the web version of this article.)

Phenomenex, Le Pecq, France) coupled with mass spectrometry (Shimadzu QP2010, Kyoto, Japan). The injection port was used in split mode (split ratio 50) at 270 °C. The carrier gas (He) velocity was constant at 35 cm.s^{-1}. The oven temperature was initially maintained at 50 °C for 1 min, then ramped up to 280 °C at a rate of 10 °C/min. The final temperature was maintained for 5 min. Mass spectra were recorded in electron ionization mode at 70 eV. The scanning range was 40 to 650 amu (atomic mass unit). The temperatures of the transfer line and ion source were maintained at 280 °C and 200 °C, respectively. Compounds were identified by comparing their mass spectra to those present in the MCF library [22], and identities were confirmed by injection of reference standards. Compounds were quantified with respect to equivalent standards.

2.4. Glucose, acetate, and protease titration

Glucose and acetate were quantified using BioSenTec kits (Auzeville Tolosane, France). Protease concentration was determined using the Pierce™ Colorimetric Protease Assay kit (Sigma Aldrich, Vienne, Austria). All kits were used according to the manufacturers' protocols.

2.5. Autolytic activity

Overnight cultures of WT and Δ*sl2*Δ*eag* mutant strains were diluted in 4 mL MODG media at an initial OD_{600nm} of 0.02. Cultures were incubated at 37 °C with shaking at 200 rpm. Once early stationary growth phase was reached, cells were washed and resuspended in 50 mM Tris-HCl buffer pH 8.5, plated in 96-well microplates and incubated at 30 °C for 15 h [23]. Optical density (OD_{600nm}) was monitored using an automated optical density reader (Flx-Xenius XMA, Safas, Monaco). The autolytic rate was expressed as the percentage decrease of OD_{600nm} after 15 h. Experiments were performed in triplicate.

2.6. Cold stress survival

Overnight cultures of WT and Δ*sl2*Δ*eag* mutant strains were inoculated in 20 mL MODG medium in 50-mL tubes at an initial OD_{600nm} of 0.02. Cultures were incubated at 37 °C with shaking (200 rpm). Once the early stationary growth phase had been reached, cultures were placed at 4 °C with shaking for up to 50 h. Numbers of viable cells were determined by plating 100 µL of 10-fold serial dilutions of cultures on LB agar plates. The colony-forming units (CFUs) were counted after incubation for 18 h at 30 °C. All experiments were performed in quadruplicate.

2.7. Salt stress

Overnight cultures of WT and Δ*sl2*Δ*eag* mutant strains were inoculated at an initial OD_{600nm} of 0.02 and incubated at 37 °C with shaking (200 rpm) in 10 mL MODG medium in 50-mL tubes. Early stationary phase cells were exposed to 5% (*w/v*) sodium chloride (NaCl) for 1 h or 2 h at 37 °C under shaking. The number of viable cells was determined by plating 100 µL of 10-fold serial dilutions of cultures on LB agar plates, and CFUs were counted after incubation for 18 h at 30 °C. All experiments were performed in triplicate.

2.8. Statistical analysis

Statistical analysis (GraphPad Prism software, version 8.0; GraphPad Software, San Diego, CA, USA) involved data from at least three biological replicates. Means were reported with standard deviations (SD). Statistical significance of differences in rate of glucose uptake and protease concentrations were evaluated using a Student's *t*-test. All other experiments were analyzed by one-way analysis of variance (ANOVA) followed by Bonferroni post hoc analysis. *p*-values ≤ 0.05 were considered significant.

2.9. Bioinformatics analysis

The subcellular localization of proteins identified in the exoproteome was predicted using several bioinformatics tools: SignalP4.1 (http://www.cbs.dtu.dk/Services/SignalP/), Phobius (http://www.ebi.ac.uk/Tools/pfa/phobius/), PSORTb v3.0.3 (https://www.psort.org/psortb/), TMHMM 2.0 (http://www.cbs.dtu.dk/services/TMHMM), and SignalP v6.0 (https://services.healthtech.dtu.dk/service.php?SignalP-6.0). Venn diagrams were produced using the Calculate and draw custom Venn diagrams tool (https://bioinformatics.psb.ugent.be/webtools/Venn/).

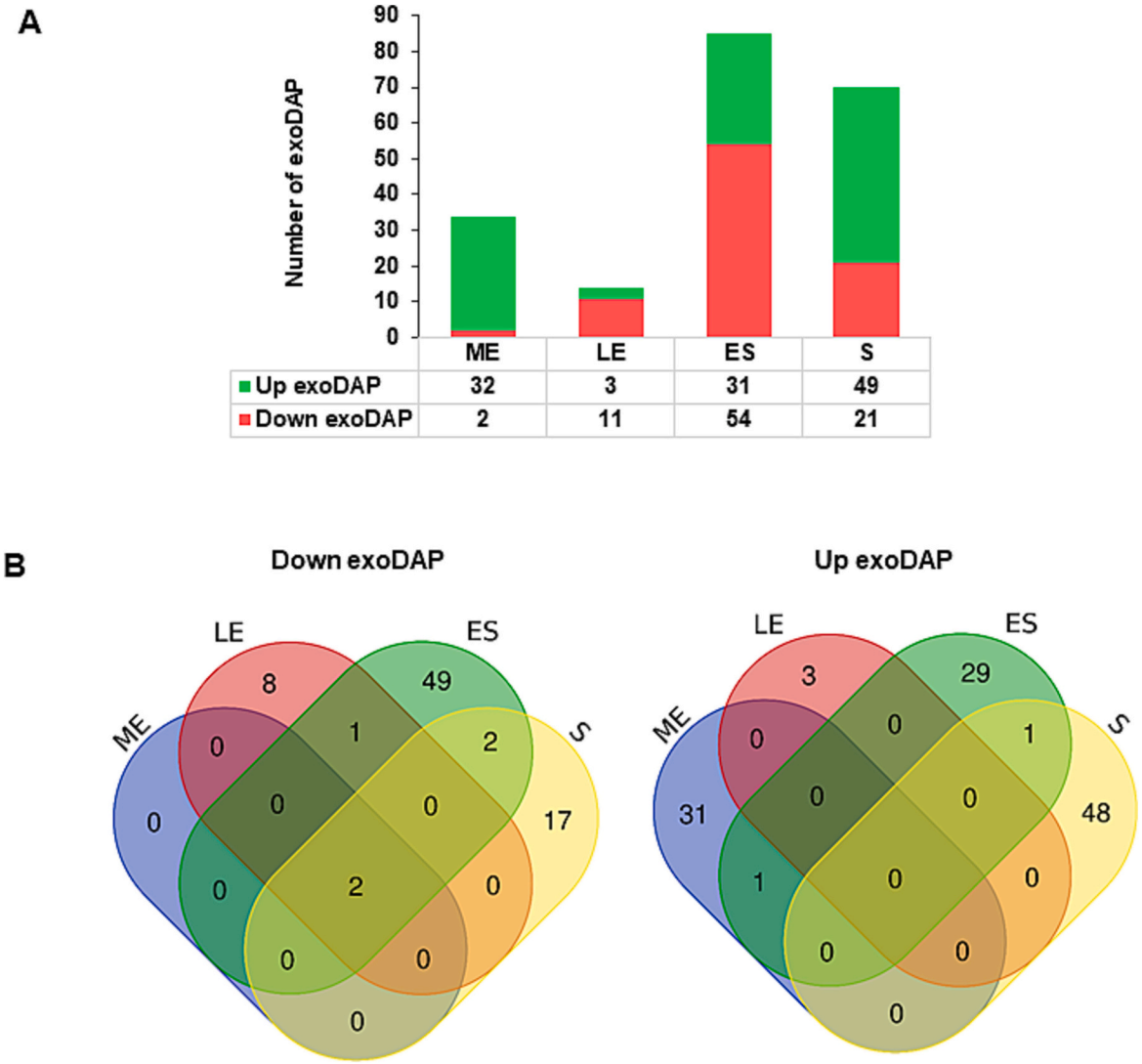

Fig. 5. Dynamics of exoproteins differentially accumulating (exoDAPs) in Δ*sl2*Δ*eag* mutant compared to WT. A. Bar chart showing up- and down-exoDAPs. The numbers of up- (green) and down- (red) exoDAPs are shown above each bar. B. Venn diagrams of down- and up-exoDAPs identified at the different time-points. (For interpretation of the references to colour in this figure legend, the reader is referred to the web version of this article.)

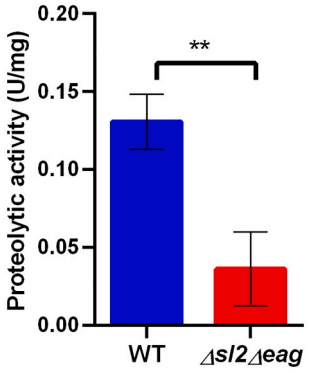

Fig. 6. Extracellular proteolytic activity in supernatants from Δ*sl2*Δ*eag* and WT cultures. Error bars represent the standard deviation from three biological triplicates. Significant differences ($p < 0.01$) are indicated by two asterisks.

3. Results

3.1. Physiological consequences of S-layer biogenesis in B. cereus AH187

The impact of S-layer synthesis on *B. cereus* AH187 physiological growth processes was investigated in chemically defined MODG medium, commonly used in studies of *B. cereus*. This growth medium, containing glucose and amino acids as carbon and energy sources [22], was chosen for its established relevance. Its defined composition ensures controlled and reproducible growth conditions, aligning with our study's objectives and enhancing comparability with prior research. In line with our previous results [3], the WT *B. cereus* AH187 and Δ*sl2*Δ*eag* mutant strains had similar growth rates ($\mu_{max} = 1.1 \pm 0.1\ h^{-1}$, and $1.0 \pm 0.1\ h^{-1}$, respectively) and biomass production (Fig. 1). We collected aliquots of culture extracts at four time-points (named ME, LE, ES, and S) over the growth curve (Fig. 1). In these aliquots, we evaluated glucose and amino acid consumption, and acetate overflow for the WT and Δ*sl2*Δ*eag* mutant strains (Fig. 2 and Fig. S1). The data showed that both the WT and Δ*sl2*Δ*eag* cultures exhibited maximal glucose uptake at the ME time-point, i.e., at the maximal growth rate. However, the glucose uptake rate was lower for the Δ*sl2*Δ*eag* mutant strain than for the parent strain. Both the WT and Δ*sl2*Δ*eag* mutant strains consumed threonine, serine,

Table 1
Soluble extracellular proteins that differentially accumulated in *Δsl2Δeag* mutant exoproteome compared to WT exoproteome.

Uniprot ID	Gene name	Description	Fold change and significance[a]							
			ME		LE		ES		S	
			log_2 FC	*p* value	log_2 FC	*p* value	log_2 FC	*p* value	log_2 FC	*p* value
B7HVL4		Immune inhibitor A	**1.00**	**0.00**	0.00	0.00	−0.74	0.06	−0.83	0.18
A1BYI0		Neutral metalloproteinase	0.46	0.47	0.12	0.34	**−0.69**	**0.05**	−0.20	0.44
B7HKT0	chi36	Extracellular exochitinase	0.00	nd[b]	0.00	nd	**−1.00**	**0.02**	−0.81	0.10
B7HQ08		Neutral metalloprotease	0.00	nd	0.00	nd	**−2.32**	**0.02**	**−1.00**	**0.02**
B7HZ26	lla2	Beta-lactamase	0.00	nd	0.00	nd	**−1.00**	**0.01**	−0.35	0.02
B7HUF7		NLP/P60 family protein	0.00	nd	0.00	nd	**−0.84**	**0.01**	−0.04	0.74
B7HVP3	adP2	Alkaline D-peptidase	0.74	0.42	−0.74	0.18	**−1.25**	**0.03**	0.20	0.38
B7HVW7		Neutral metalloproteinase	0.74	0.42	0.04	0.87	**−1.01**	**0.05**	−0.04	0.85
B7HW99	sph	Sphingomyelin phosphodiesterase	0.58	0.44	0.19	0.50	**−0.67**	**0.04**	−0.74	0.15
B7I0J0	inhA1	Immune inhibitor A metalloprotease	−0.16	0.88	0.00	1.00	**−1.39**	**0.05**	−0.10	0.81
B7HVA4		Neutral metalloproteinase	0.72	0.45	0.49	0.42	−1.05	0.07	**−1.16**	**0.03**

[a] The log_2 fold-change (log_2FC) was determined using PatternLab software at mid-exponential (ME), late exponential (LE), early stationary (ES), and stationary (S) growth phases. Plus and minus symbols indicate up- and down-accumulation of the proteins, respectively. Numbers in bold indicate that data satisfied both log_2FC ($\leq$0.46 and $\geq$0.46) and statistical criteria (*p* value$\leq$0.05).
[b] ND: not determined.

isoleucine, and valine from the beginning of growth, and phenylalanine, tyrosine, methionine, lysine, and glutamic acid after 5 h of growth (Fig. S1). The Δ*sl2*Δ*eag* mutant strain consumed glycine and aspartic acid earlier than the WT strain (at the ME rather than the LE time-point, Fig. 2). Acetate overflow was unchanged in the mutant strain compared to the WT (Fig. S1). Taken together, these data indicate that *B. cereus* circumvents the metabolic cost of S-layer synthesis by accelerating highly energy-efficient glucose catabolism at the expense of low energy-efficiency amino acid catabolism.

3.2. Comprehensive analysis of cellular proteome remodeling in Δsl2Δeag cells

To investigate the metabolic consequences of S-layer synthesis, we compared the cellular proteomes of WT and Δ*sl2*Δ*eag* cells collected at ME, LE, ES, and S time-points (Fig. 1). In total, 2329 cellular proteins were identified by at least two distinct peptides across all 24 samples analyzed (2 strains × 3 biological replicates × 4 time-points, Table S1). Principal component analysis (PCA) revealed good homogeneity of the biological triplicates for the two strains at each time-point, and distinguished the four time-points (Fig. S2).

Differential analysis identified 309 proteins with significantly different abundances (|log*2* fold-change| $\geq$ 0.46, *p*-value $\leq$0.05, Table S2) in Δ*sl2*Δ*eag* compared to WT. Among these, 117 proteins were detected at lower levels in Δ*sl2*Δ*eag* compared to WT (down-DAPs), whereas 192 were detected at higher levels (up-DAPs) (Table S2). The growth phase distribution of down- and up-DAPs is illustrated in Fig. 3, revealing that (i) the number of DAPs increased during growth and reached its maximum at the transition between exponential and stationary growth (ES, Fig. 3A), (ii) at every time-point, up-DAPs outnumbered down-DAPs, and (iii) time-points shared few DAPs (Fig. 3B). The two down-DAPs identified in all time-points (Fig. 3B) are the S-layer proteins SL2 and EA1, which were undetectable in the Δ*sl2*Δ*eag* cellular proteome, as expected (Table S1). Taken together, these data indicate that the lack of SL2 and EA1 synthesis in Δ*sl2*Δ*eag* cells is accompanied by a growth-phase-dependent remodeling of the cellular proteome. We next focused our attention on the changes occurring at each time-point (Table S2).

3.2.1. ME time-point

In addition to SL2 and EA1, only two down-DAPs were identified at the mid-exponential growth phase. One of these was the putative transition state transcriptional regulatory protein B7HND9, which could regulate growth-phase dependent processes in the same way as its counterparts, AbrB and AbrB' [24]. The 19 up-DAPs included two components of signal transduction pathways: (i) YycH (B7HZF1), which controls the activity of the YycFG two-component system, essential for cell wall homeostasis, cell membrane integrity, and cell division in *B. subtilis* [25], and (ii) B7HLT0, a putative CheY chemotaxis response regulator [26]. Interestingly, B7HLT0 abundance was also increased in the Δ*sl2*Δ*eag* mutant strain at the LE and ES time-points, suggesting that lack of S-layer synthesis could up-regulate the chemotaxis transduction pathway during exponential growth.

3.2.2. LE time-point

Few down-DAPs were identified compared to up-DAPs and were divided across several functional groups (Fig. 4). The majority of up-DAPs were clustered in functional groups corresponding to post-translational modification/chaperone/defense mechanisms [N], transcription [T] and translation [S]. They included: (i) the co-chaperonin GroES (B7HS04), the putative heat shock protein B7HQ56, and the cold-shock protein CspB2 (B7HZX9) that help with folding of nascent proteins, and the refolding and degradation of misfolded proteins, (ii) the protein SufA (B7HUW9) and the NifU-like protein B7HUU3 that contributes to iron-sulfur cluster assembly, and (iii) the RNA chaperone Hfq (B7HKR8) and the methionine sulfoxide reductase MsrA (B7HMM2) that help to maintain the cell's redox status [27]. The 13 up-DAPs classified in transcription and translation categories included RNA polymerase subunit Y (RpoY, B7HMU7), transcription elongation and termination factors, five transcriptional regulators, and translational ribosomal subunits (Table S2). Taken together these data suggest that (i) cellular processes associated with growth are more active in Δ*sl2*Δ*eag* than in WT cells, and (ii) increased activity of growth-related processes in Δ*sl2*Δ*eag* cells is associated with increased cellular stress response.

3.2.3. ES time-point

This time-point characterizes the shift from exponential growth to the stationary phase, and marks the initiation of the sporulation process. Fig. 4 shows that up-DAPs were overrepresented in categories related to active growth, i.e., post-translational modification/chaperone/defense mechanisms [N] and nucleotide [M] transport and metabolism, [S] and [T] categories. The down-DAPs were overrepresented in the amino acid [A], replication/recombination [O], [N], and sporulation [R] categories. The down-DAPs in category [A] included five proteins (LeuA, LeuB, IlvB, IlvC, and IlvE1) involved in branched-chain amino acid (BCAA) synthesis. These proteins are all encoded by the *ilv-leu* operon, which is regulated by multiple general regulators triggered by BCAA, carbon, and nitrogen availability [28]. The down-DAPs classed in the [O], [N], and [R] categories included: (i) co-chaperone GroES and aminopeptidases in the M42 (B7HSN1) and M20 (B7HYH6) families, which can aid in the

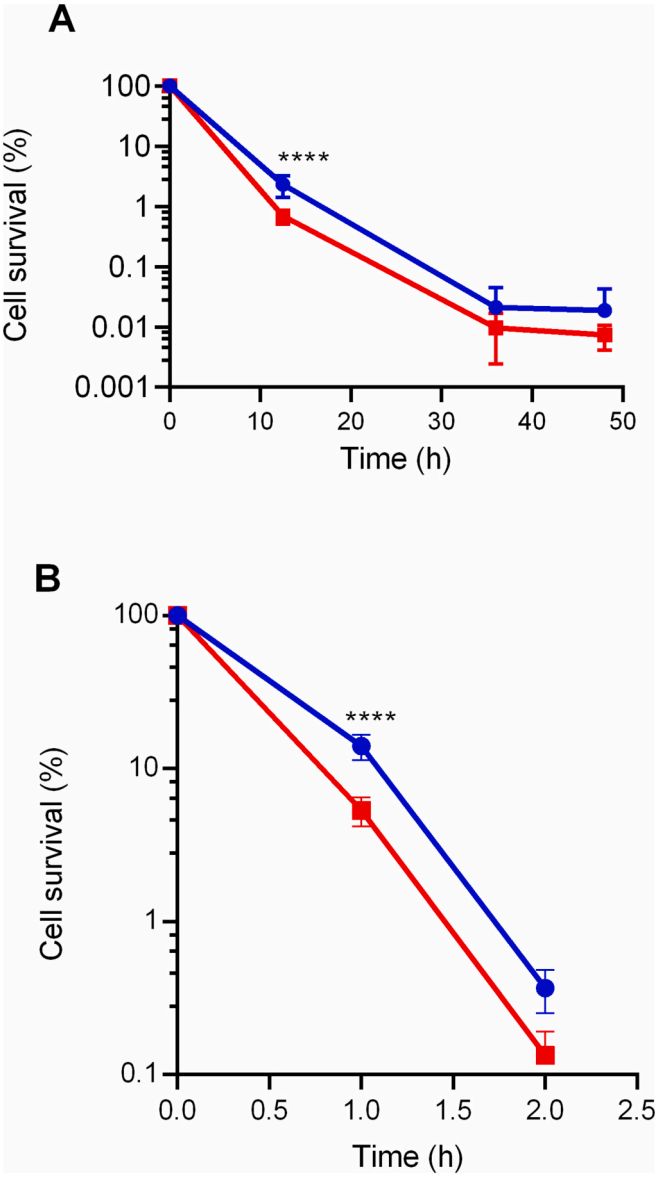

Fig. 7. Survival of stationary Δ*sl2*Δ*eag* and WT cells in abiotic stress conditions. A. Survival rate upon exposure to cold. B. Survival rate in 5% NaCl. Survival rates of Δ*sl2*Δ*eag* (red) and WT (blue) cells are expressed as (*N*/*N*0) × 100. *N*0 is the initial number of CFUs, and *N* is the number of CFUs detected after the stress treatment. The data correspond to the mean from three biological replicates. Error bars represent the mean standard deviations for the data points. Statistical analysis was based on one-way ANOVA followed by Bonferroni's post hoc analysis. **: $p < 0.01$, ****: $p < 0.0001$. (For interpretation of the references to colour in this figure legend, the reader is referred to the web version of this article.)

degradation of misfolded proteins, (ii) MutL (B7HLA2), UvrB (B7HWZ4), and RecJ (B7HQG8), involved in regulatory systems to cope with DNA damage upon entry into the stationary phase, and (iii) sigma factors σE and σF, anti-sigma SpoIIAB (B7HN54) and anti-anti-sigma factor SpoIIAA (B7HN53), which are involved in spore development and activation of the sporulation machinery [29–31] (Table S2). Taken together, these data indicate that the Δ*sl2*Δ*eag* mutations perturb the metabolic reprogramming that sustains the shift from active growth to starvation and entry into sporulation. In line with this perturbation, we observed that catalase KatB (B7HZT0) and DNA protection during starvation protein 2 Dps2 (B7HVX5) – which both protect bacterial cells against many different types of stressors, including starvation – were down-regulated in the Δ*sl2*Δ*eag* mutant strain (Table S2). Other down-regulated proteins included the molybdopterin biosynthesis co-factor MoeB (B7HW37) that contributes to maintaining intracellular sulfur and thiol homeostasis and prevents ROS damage [32], four proteins involved in the bacillibactin biosynthesis pathway, and three proteins implicated in iron-transport. In contrast, the organic hydroperoxide resistance protein, (OhrR, [32]) and the bacterioferritin comigratory protein Bcp (B7HU71) [33], which protect cells against peroxide stress accumulated in mutant cells. These data clearly indicate that, faced with oxidative stress and iron starvation, at the entry to the stationary phase, the Δ*sl2*Δ*eag* mutant reacts differently to the WT strain.

3.2.4. *S time-point*

Proteome remodeling throughout the stationary phase (between the ES and S time-points) was accompanied by a decrease in the number of DAPs (Fig. 3A). The six down-DAPs identified at both ES and S time-points included the BCAA biosynthesis-related proteins IlvC1, LeuA, and LeuB (Table S2). The 11 down-DAPs that were specific to the S time-point included the sugar-binding transcriptional regulator LacI (B7HNX4), which could act as a repressor of carbon catabolism [34]. Up-DAPs included the cellular stress-related protein Bcp, previously identified at the ES time-point, and two proteins involved in transcriptional regulation: the σ_H transcriptional factor (B7HQ58), involved in stress adaptation, toxin gene expression and spore formation [35,36]; and the transcriptional regulator MntR (B7HNW6), regulating manganese transport [37]. In conclusion, the difference in metabolic reprogramming occurring at the early stationary phase in Δ*sl2*Δ*eag* cells compared to WT tended to attenuate during the stationary phase.

3.3. *Exoproteome remodeling in Δsl2Δeag cells*

To complete the information obtained from the cellular proteome, we examined the impact of defective S-layer synthesis on the *B. cereus* exoproteome over time. A total of 1781 proteins were identified by at least two peptides (Table S3) in the 24 samples analyzed (Fig. S2). Comparison of the *Δsl2Δeag* mutant to the WT identified 192 proteins with differential abundances (exoDAPs) (Table S4). Fig. 5A shows how the 79 down-exoDAPs and the 113 up-exoDAPs distributed over time. The majority of down-exoDAPs was identified at the ES time-point, whereas the up-exoDAPs were shared across the ME, ES, and S time-points. Very few proteins were detected at more than one time-point (3/79 down-exoDAPS and 5/113 up-exoDAPs), and only SL2 and EA1 were differentially accumulated in all four time-points (down-exoDAPs, Fig. 5B). This observation suggests that the *Δsl2Δeag* mutations induced remodeling of the *B. cereus* AH187 exoproteome in a growth-phase-dependent manner, similar to their effects on the cellular proteome.

The proteins identified in the exoproteome of *B. cereus* were true extracellular proteins, cell surface proteins, and proteins derived from cell lysis during culture and harvest [38]. Prediction of the subcellular localizations of the 192 exoDAPs indicated that 11 were soluble extracellular proteins and 50 were cell wall/surface-associated proteins (Table S4). The 11 soluble extracellular proteins corresponded to degradative enzymes, the majority of which were detected at lower levels in the *Δsl2Δeag* mutant ES exoproteome than in the WT ES proteome (Table 1). To determine whether decreased protease abundance in the *Δsl2Δeag* mutant strain correlated with an overall decrease in extracellular proteolytic activity, we compared protease activity between WT and *Δsl2Δeag* mutant cells. Fig. 6 shows that extracellular proteolytic activity was indeed lower for the *Δsl2Δeag* mutant than for the WT strain, confirming our assumption. Thus, lack of S-layer synthesis affects the proteolytic response upon entry into the stationary phase.

3.4. *Resistance to osmotic and cold stress*

The bacterial stationary/starvation response provides protection

against abiotic stressors such as osmotic shock and temperature variations [39]. Our proteomics data suggested a defect in the stationary/starvation response in the Δ*sl2*Δ*eag* mutant strain. To confirm this, we compared the ability of the Δ*sl2*Δ*eag* mutant and WT strains to survive NaCl-mediated osmotic stress and low temperature following entry into the stationary phase. The results showed that the Δ*sl2*Δ*eag* mutant strain was less resistant to both cold temperature (Fig. 7A), and 5% (*w/v*) salt stress (Fig. 7B) than the WT strain, indicating a defect in general protection.

4. Discussion

The aim of this study was to determine how production of the S-layer influenced *B. cereus* metabolism at various stages of the growth curve, based on its effects on the cellular proteome and exoproteome. By utilizing a conventional data-dependent acquisition strategy and the Q-Exactive HF tandem mass spectrometer, we successfully identified a collective of 2550 *B. cereus* cellular- and *exo*-proteins from an estimated 5783 open reading frames (ORFs). This results in a protein coverage of approximately 44%. When comparing this protein coverage to recent *B. cereus* cellular and spore proteome data [40] [41], our findings align closely with the reported trends.

The entry of bacteria into the stationary phase can be caused by a number of factors, including limitation of a specific essential nutrient, accumulation of toxic by-products and exposure to stress factors [39]. Stationary phase survival strategies include numerous physiological, metabolic, and morphological changes, which are regulated by interconnected signaling pathways [39]. We previously showed that the *B. cereus* AH187 S-layer was enriched in both SL2 and EA1 SLPs when growing cells entered the stationary phase, and that the S-layer improves the capacity of starved *B. cereus* AH187 cells to adhere to abiotic surfaces [16]. Although energetically costly, synthesis of the S-layer has no detrimental effect on *B. cereus* AH187 growth in defined MODG medium. However, the results presented here show that S-layer synthesis affects carbon/energy metabolism during the early stages of growth, and triggers extensive proteome remodeling upon entry into the stationary phase. To address potential genetic adaptation concerns, we have taken meticulous steps to ensure the consistency of the observed proteomic changes across various growth stages. This careful approach reinforces our conclusion that these proteomic alterations primarily emanate from the absence of the S-layer and its direct ramifications for bacterial physiology.

MODG medium contains both glucose and amino acids, which are rapidly consumed by *B. cereus* at the beginning of growth to cover the high catabolic and anabolic demands [42]. Our data indicate that WT cells require a faster glucose uptake rate than *Δsl2Δeag* mutant cells, and thus generate ATP more rapidly through glycolysis. The increased glucose uptake rate in WT cells was associated with decreased low-cost amino acid uptake, in particular of glycine and aspartate. Taken together, these data indicate that S-layer synthesis, probably due to its energy requirement, alters the coordination of glucose and amino acid catabolism [43–45].

Entry into the stationary phase elicits changes in protein abundance that considerably remodel the proteome [27,46]. This remodeling affects a wide range of biological processes and response mechanisms, leading to decreased abundance of proteins needed for exponential growth, and increased abundance of proteins improving the bacteria's ability to detect and take up nutrients, protecting cells against stress, and allowing efficient adaptation under persistently unfavorable conditions [39,47]. The differences in reorganization of the ES proteome in *Δsl2Δeag* and WT cells suggest that S-layer synthesis modulates the stationary phase response. Proteome changes in *Δsl2Δeag* cells compared to WT involved general stress proteins belonging to the σB regulon [48], such as catalase (KatK), the DNA-protecting enzyme Dps2, proteins repairing oxidative damage (Ohr, MoeB, Bcp), DNA-repair proteins (MutL, UvrB, RecJ), and chaperones (GroES and proteins from the M42 and M40 families). Some of these proteins (KatB, Dsp2, GroES) are also known to be regulated by CcpA [49], by the histidine-containing protein Hpr [50], and by RpoE ([48] (Table S3). The BCAA proteins – encoded by the *ilv-leu* operon, controlled by CcpA and CodY [55,56] – were less abundant in the *Δsl2Δeag* mutant compared to the WT strain. Several proteolytic enzymes, as well as the σF and σE sporulation factors, which were also less abundant in the proteome of the *Δsl2Δeag* mutant strain, are transcriptionally controlled by Spo0A. We conclude that S-layer synthesis modulates the stationary response by instructing the interconnected regulons σB, CcpA, CodY, and Spo0A to control the nutrient starvation and general stress responses.

How does S-layer synthesis modulate the stationary phase response? The metabolic cost of S-layer synthesis is probably higher upon entry into the stationary phase than during the exponential phase, since the S-layer is enriched with SLPs during growth [3]. At the beginning of exponential growth, bacteria focus on maximizing their growth rate, and due to the high availability of carbon/energy sources, they deal with the "low" metabolic cost of S-layer synthesis by re-routing carbon without significantly reorganizing the proteome. Upon entry into the stationary phase, bacteria focus on surviving in the face of starvation. Due to the large increase in biomass/energy required to maintain the S-layer, they must also minimize the number of active processes though a major proteome reorganization orchestrated by regulators reacting to nutrient and energy status. By maximizing the stationary response, S-layer-producing *B. cereus* cells maximize fitness in starvation conditions since: (i) they are more resistant to abiotic stresses such as osmotic stress and low temperatures, and (ii) they secrete proteolytic enzymes in higher amounts, which can help them to retrieve nutrients by recycling organic material from dead biomass and debris. Finally, in MODG medium, the metabolic cost of S-layer synthesis may act as a stress factor to trigger an efficient adaptive stationary/starvation response, driven by the general regulators reacting to energy and nutrient status.

Upon entry into the stationary phase, bacteria remodel their proteome and increase the synthesis of specific stationary phase proteins. The S-layer protein EA1, in contrast to SL2 could be an "inducible stationary phase" protein, since it mainly accumulates during this phase of growth. The genes encoding SL2 and EA1 (*sl2* and *eag*, respectively), are both regulated by Spo0A [11]. A CodY binding site was identified in the promoter regions of *eag* (data not shown), suggesting that *eag* is repressed by CodY. A similar interaction is reported for the orthologs of these two genes in *B. anthracis* (*sap* and *eag*) [57]. Interestingly, we also identified a potential CcpA binding site in the *sl2* promoter region [10] and a σH binding site in the promoter region of *eag* (data not shown), suggesting that *eag*, in contrast to *sl2*, may be a member of the σ_H-inducible branch of the *B. cereus* stationary response. However, we cannot exclude that inducible stationary phase expression of *eag* also results from its repression by SL2, as reported for SAP in *B. anthracis* [58]. Finally, SL2 and EA1 are unquestionably involved in the stationary/starvation response.

The synthesis of SLPs, like SL2 and EA1, that protect bacteria, and increase their survival chances upon starvation, comes at the expense of the synthesis of proteins needed for growth. The result is a trade-off between a fitness cost during growth and a fitness benefit in starvation conditions. Trade-offs prevent ecological fitness in all environments [59]. We can thus speculate that the S-layer-related trade-off may constrain emetic *B. cereus*, and other S-layer-producing *B. cereus* strains to specific environments, where the fitness cost during growth is low. The inquiry into the natural reservoir for emetic *B. cereus* strains gains relevance within this context. The potential fitness trade-off associated with S-layer production suggests that these strains might thrive better in environments where nutrients are less abundant. In this regard, root and tuber vegetables emerge as likely niches that align with this trade-off scenario. These environments provide a steady nutrient supply while potentially constraining rapid bacterial proliferation. The intricate surfaces of root and tuber vegetables, combined with varying nutrient availability, may resemble the conditions driving the trade-off dynamics

seen in controlled laboratory settings. Therefore, considering root and tuber vegetables as potential natural reservoirs for emetic *B. cereus* strains seems plausible [2]. It is noteworthy that our study targeted a mutant strain deficient in both EA1 and SL2 synthesis. Regrettably, the construction of a mutant specifically targeting only EA1 was hindered by technical limitations [3]. Nonetheless, this limitation doesn't diminish the value of our exploration into the roles of both SL2 and EA1 SLPs, offering essential insights into their potential functions and ecological significance. The concurrent presence of two distinct SLPs potentially amplifies the adaptive capabilities of emetic *B. cereus* strains within specific environments. Each S-layer protein likely endows unique advantages, augmenting the strain's competitive prowess, survivability, and resource utilization. To enhance our comprehension, it becomes imperative to examine growth conditions closely resembling root and tuber environments. Investigating how emetic *B. cereus* strains, particularly *B. cereus* AH187, respond to varying nutrient levels, physical structures, and interactions within these conditions could yield profound insights into their potential habitats and adaptive strategies. This interplay between nutrient availability, specific S-layer proteins, and fitness trade-offs presents a promising avenue for future research, deepening our understanding of the ecological niche and evolutionary dynamics."

Supplementary data to this article can be found online at https://doi.org/10.1016/j.jprot.2023.105007.

Declaration of Competing Interest

The authors declare no conflict of interest.

Data availability

No

Acknowledgments

We thank Claire Dargaignaratz for her efficient technical help. CB's PhD work was supported by a fellowship from the French Ministry for Research and Higher Education (Ministère de la Recherche et de l'Enseignement Supérieur). This work was partly supported by a grant from Avignon University.

References

[1] R. Dietrich, N. Jessberger, M. Ehling-Schulz, E. Märtlbauer, P.E. Granum, The food poisoning toxins of *Bacillus cereus*, Toxins. 13 (2021) 98, https://doi.org/10.3390/toxins13020098.

[2] M. Ehling-Schulz, E. Frenzel, M. Gohar, Food–bacteria interplay: pathometabolism of emetic *Bacillus cereus*, Front. Microbiol. 6 (2015). https://www.frontiersin.org/articles/10.3389/fmicb.2015.00704 (accessed August 18, 2023).

[3] C. Boutonnet, S. Lyonnais, B. Alpha-Bazin, J. Armengaud, A. Château, C. Duport, Dynamic profile of S-layer proteins controls surface properties of emetic *Bacillus cereus* AH187 strain, Front. Microbiol. 13 (2022). https://www.frontiersin.org/articles/10.3389/fmicb.2022.937862 (accessed February 9, 2023).

[4] D. Missiakas, O. Schneewind, Assembly and function of the *Bacillus anthracis* S-layer, Annu. Rev. Microbiol. 71 (2017) 79–98, https://doi.org/10.1146/annurev-micro-090816-093512.

[5] T.A.M. Bharat, A. von Kügelgen, V. Alva, Molecular logic of prokaryotic surface layer structures, Trends Microbiol. 29 (2021) 405–415, https://doi.org/10.1016/j.tim.2020.09.009.

[6] D. Pum, A. Breitwieser, U.B. Sleytr, Patterns in nature—S-layer lattices of bacterial and archaeal cells, Crystals. 11 (2021) 869, https://doi.org/10.3390/cryst11080869.

[7] J. Ravi, A. Fioravanti, S-layers: the proteinaceous multifunctional armors of gram-positive pathogens, Front. Microbiol. 12 (2021) 663468, https://doi.org/10.3389/fmicb.2021.663468.

[8] R.P. Fagan, N.F. Fairweather, Biogenesis and functions of bacterial S-layers, Nat. Rev. Microbiol. 12 (2014) 211–222, https://doi.org/10.1038/nrmicro3213.

[9] M. Sára, U.B. Sleytr, S-layer proteins, J. Bacteriol. 182 (2000) 859–868, https://doi.org/10.1128/jb.182.4.859-868.2000.

[10] C. Duport, L. Rousset, B. Alpha-Bazin, J. Armengaud, *Bacillus cereus* decreases NHE and CLO exotoxin synthesis to maintain appropriate proteome dynamics during growth at low temperature, Toxins. 12 (2020) 645, https://doi.org/10.3390/toxins12100645.

[11] L. Rousset, B. Alpha-Bazin, A. Château, J. Armengaud, T. Clavel, O. Berge, C. Duport, Groundwater promotes emergence of asporogenic mutants of emetic *Bacillus cereus*, Environ. Microbiol. 22 (2020) 5248–5264, https://doi.org/10.1111/1462-2920.15203.

[12] M. Isalan, C. Lemerle, K. Michalodimitrakis, C. Horn, P. Beltrao, E. Raineri, M. Garriga-Canut, L. Serrano, Evolvability and hierarchy in rewired bacterial gene networks, Nature. 452 (2008) 840–845, https://doi.org/10.1038/nature06847.

[13] E. Rosenfeld, C. Duport, A. Zigha, P. Schmitt, Characterization of aerobic and anaerobic vegetative growth of the food-borne pathogen *Bacillus cereus* F4430/73 strain, Can. J. Microbiol. 51 (2005) 149–158, https://doi.org/10.1139/w04-132.

[14] J. Armengaud, J.A. Christie-Oleza, G. Clair, V. Malard, C. Duport, Exoproteomics: exploring the world around biological systems, Expert Rev. Proteomics 9 (2012) 561–575, https://doi.org/10.1586/epr.12.52.

[15] P.C. Turnbull, J.M. Kramer, K. Jørgensen, R.J. Gilbert, J. Melling, Properties and production characteristics of vomiting, diarrheal, and necrotizing toxins of *Bacillus cereus*, Am. J. Clin. Nutr. 32 (1979) 219–228, https://doi.org/10.1093/ajcn/32.1.219.

[16] C. Boutonnet, S. Lyonnais, B. Alpha-Bazin, J. Armengaud, A. Château, C. Duport, Dynamic profile of S-layer proteins controls surface properties of emetic *Bacillus cereus* AH187 strain, Front. Microbiol. 13 (2022). https://www.frontiersin.org/article/10.3389/fmicb.2022.937862 (accessed July 1, 2022).

[17] J.-P. Madeira, B. Alpha-Bazin, J. Armengaud, C. Duport, Time dynamics of the *Bacillus cereus* exoproteome are shaped by cellular oxidation, Front. Microbiol. 6 (2015) 342, https://doi.org/10.3389/fmicb.2015.00342.

[18] E.M. Hartmann, J. Armengaud, Shotgun proteomics suggests involvement of additional enzymes in dioxin degradation by *Sphingomonas wittichii* RW1, Environ. Microbiol. 16 (2014) 162–176, https://doi.org/10.1111/1462-2920.12264.

[19] V. Dupierris, C. Masselon, M. Court, S. Kieffer-Jaquinod, C. Bruley, A toolbox for validation of mass spectrometry peptides identification and generation of database: IRMa, Bioinformatics. 25 (2009) 1980–1981, https://doi.org/10.1093/bioinformatics/btp301.

[20] J.A. Christie-Oleza, B. Fernandez, B. Nogales, R. Bosch, J. Armengaud, Proteomic insights into the lifestyle of an environmentally relevant marine bacterium, ISME J. 6 (2012) 124–135, https://doi.org/10.1038/ismej.2011.86.

[21] P.C. Carvalho, J.R. Yates III, V.C. Barbosa, Improving the TFold test for differential shotgun proteomics, Bioinformatics. 28 (2012) 1652–1654, https://doi.org/10.1093/bioinformatics/bts247.

[22] S.G. Villas-Bôas, K.F. Smart, S. Sivakumaran, G.A. Lane, Alkylation or silylation for analysis of amino and non-amino organic acids by GC-MS? Metabolites. 1 (2011) 3–20, https://doi.org/10.3390/metabo1010003.

[23] N. Raddadi, A. Cherif, D. Mora, L. Brusetti, S. Borin, A. Boudabous, D. Daffonchio, The autolytic phenotype of the *Bacillus cereus* group, J. Appl. Microbiol. 99 (2005) 1070–1081, https://doi.org/10.1111/j.1365-2672.2005.02713.x.

[24] G. Lücking, M.K. Dommel, S. Scherer, A. Fouet, M., Ehling-Schulz, Cereulide synthesis in emetic *Bacillus cereus* is controlled by the transition state regulator AbrB, but not by the virulence regulator PlcR, Microbiology. 155 (2009) (2009) 922–931, https://doi.org/10.1099/mic.0.024125-0.

[25] H. Szurmant, M.A. Mohan, P.M. Imus, J.A. Hoch, YycH and YycI interact to regulate the essential YycFG two-component system in *Bacillus subtilis*, J. Bacteriol. 189 (2007) 3280–3289, https://doi.org/10.1128/JB.01936-06.

[26] T. Schweinitzer, C. Josenhans, Bacterial energy taxis: a global strategy? Arch. Microbiol. 192 (2010) 507–520, https://doi.org/10.1007/s00203-010-0575-7.

[27] J.-P. Madeira, B.M. Alpha-Bazin, J. Armengaud, C. Duport, Methionine residues in exoproteins and their recycling by methionine sulfoxide reductase AB Serve as an antioxidant strategy in *Bacillus cereus*, Front. Microbiol. 8 (2017). https://www.frontiersin.org/article/10.3389/fmicb.2017.01342 (accessed May 14, 2022).

[28] R.P. Shivers, A.L. Sonenshein, *Bacillus subtilis* ilvB operon: an intersection of global regulons, Mol. Microbiol. 56 (2005) 1549–1559, https://doi.org/10.1111/j.1365-2958.2005.04634.x.

[29] M. Fujita, R. Losick, An investigation into the compartmentalization of the sporulation transcription factor σE in *Bacillus subtilis*, Mol. Microbiol. 43 (2002) 27–38, https://doi.org/10.1046/j.1365-2958.2002.02732.x.

[30] C. Karmazyn-Campelli, L. Rhayat, R. Carballido-López, S. Duperrier, N. Frandsen, P. Stragier, How the early sporulation sigma factor σF delays the switch to late development in *Bacillus subtilis*, Mol. Microbiol. 67 (2008) 1169–1180, https://doi.org/10.1111/j.1365-2958.2008.06121.x.

[31] P.J. Lewis, T. Magnin, J. Errington, Compartmentalized distribution of the proteins controlling the prespore-specific transcription factor σF of *Bacillus subtilis*, Genes Cells 1 (1996) 881–894, https://doi.org/10.1046/j.1365-2443.1996.750275.x.

[32] M. Das, A. Dewan, S. Shee, A. Singh, The multifaceted bacterial cysteine desulfurases: from metabolism to pathogenesis, Antioxidants. 10 (2021) 997, https://doi.org/10.3390/antiox10070997.

[33] G. Clair, A. Lorphelin, J. Armengaud, C. Duport, OhrRA functions as a redox-responsive system controlling toxinogenesis in *Bacillus cereus*, J. Proteome 94 (2013) 527–539, https://doi.org/10.1016/j.jprot.2013.10.024.

[34] T.M. Henkin, The role of the CcpA transcriptional regulator in carbon metabolism in *Bacillus subtilis*, FEMS Microbiol. Lett. 135 (1996) 9–15, https://doi.org/10.1111/j.1574-6968.1996.tb07959.x.

[35] E. Dubnau, J. Weir, G. Nair, L. Carter, C. Moran, I. Smith, *Bacillus* sporulation gene *spo0H* codes for sigma 30 (sigma H), J. Bacteriol. 170 (1988) 1054–1062, https://doi.org/10.1128/jb.170.3.1054-1062.1988.

[36] M. Hadjifrangiskou, Y. Chen, T.M. Koehler, The alternative sigma factor σH is required for toxin gene expression by *Bacillus anthracis*, J. Bacteriol. 189 (2007) 1874–1883, https://doi.org/10.1128/JB.01333-06.

[37] M.Y. Lee, D.W. Lee, H.K. Joo, K.H. Jeong, J.Y. Lee, Structural analysis of the manganese transport regulator MntR from *Bacillus halodurans* in apo and

manganese bound forms, PLoS One 14 (2019), e0224689, https://doi.org/10.1371/journal.pone.0224689.
[38] J. Armengaud, J.A. Christie-Oleza, G. Clair, V. Malard, C. Duport, Exoproteomics: exploring the world around biological systems, Expert Rev. Proteomics 9 (2012) 561–575, https://doi.org/10.1586/epr.12.52.
[39] J. Jaishankar, P. Srivastava, Molecular basis of stationary phase survival and applications, Front. Microbiol. 8 (2017) 2000, https://doi.org/10.3389/fmicb.2017.02000.
[40] C. Mappa, O. Pible, J. Armengaud, B. Alpha-Bazin, Assessing the ratio of *Bacillus* spores and vegetative cells by shotgun proteomics, Environ. Sci. Pollut. Res. Int. 28 (2021) 25107–25115, https://doi.org/10.1007/s11356-018-3341-z.
[41] M. Abele, E. Doll, F.P. Bayer, C. Meng, N. Lomp, K. Neuhaus, S. Scherer, B. Kuster, C. Ludwig, Unified workflow for the rapid and in-depth characterization of bacterial proteomes, Mol. Cell. Proteomics 22 (2023) 100612, https://doi.org/10.1016/j.mcpro.2023.100612.
[42] E. Rosenfeld, C. Duport, A. Zigha, P. Schmitt, Characterization of aerobic and anaerobic vegetative growth of the food-borne pathogen *Bacillus cereus* F4430/73 strain, Can. J. Microbiol. 51 (2005) 149–158, https://doi.org/10.1139/w04-132.
[43] S. Laouami, K. Messaoudi, F. Alberto, T. Clavel, C. Duport, Lactate dehydrogenase a promotes communication between carbohydrate catabolism and virulence in *Bacillus cereus*, J. Bacteriol. 193 (2011) 1757–1766, https://doi.org/10.1128/JB.00024-11.
[44] J. Stülke, W. Hillen, Regulation of carbon catabolism in *Bacillus* species, Annu. Rev. Microbiol. 54 (2000) 849–880, https://doi.org/10.1146/annurev.micro.54.1.849.
[45] M. Zampieri, M. Hörl, F. Hotz, N.F. Müller, U. Sauer, Regulatory mechanisms underlying coordination of amino acid and glucose catabolism in *Escherichia coli*, Nat. Commun. 10 (2019) 3354, https://doi.org/10.1038/s41467-019-11331-5.
[46] F. Hamitouche, J. Armengaud, L. Dedieu, C. Duport, Cysteine proteome reveals response to endogenous oxidative stress in *Bacillus cereus*, Int. J. Mol. Sci. 22 (2021) 7550, https://doi.org/10.3390/ijms22147550.
[47] J. Dworkin, C.S. Harwood, Metabolic reprogramming and longevity in quiescence, Annu. Rev. Microbiol. 76 (2022) 91–111, https://doi.org/10.1146/annurev-micro-041320-111014.
[48] M. Hecker, U. Völker, General stress response of *Bacillus subtilis* and other bacteria, in: Adv. Microb. Physiol., Academic Press, 2001, pp. 35–91, https://doi.org/10.1016/S0065-2911(01)44011-2.
[49] B. Voigt, L.T. Hoi, B. Jürgen, D. Albrecht, A. Ehrenreich, B. Veith, S. Evers, K.-H. Maurer, M. Hecker, T. Schweder, The glucose and nitrogen starvation response of *Bacillus licheniformis*, PROTEOMICS. 7 (2007) 413–423, https://doi.org/10.1002/pmic.200600556.
[50] M.A. Schumacher, G.S. Allen, M. Diel, G. Seidel, W. Hillen, R.G. Brennan, Structural basis for allosteric control of the transcription regulator CcpA by the phosphoprotein HPr-Ser46-P, Cell. 118 (2004) 731–741, https://doi.org/10.1016/j.cell.2004.08.027.
[55] A.L. Sonenshein, Control of key metabolic intersections in *Bacillus subtilis*, Nat. Rev. Microbiol. 5 (2007) 917–927, https://doi.org/10.1038/nrmicro1772.
[56] S. Tojo, T. Satomura, K. Morisaki, J. Deutscher, K. Hirooka, Y. Fujita, Elaborate transcription regulation of the *Bacillus subtilis ilv-leu* operon involved in the biosynthesis of branched-chain amino acids through global regulators of CcpA, CodY and TnrA, Mol. Microbiol. 56 (2005) 1560–1573, https://doi.org/10.1111/j.1365-2958.2005.04635.x.
[57] A. Château, W. van Schaik, P. Joseph, L.D. Handke, S.M. McBride, F.M.H. Smeets, A.L. Sonenshein, A. Fouet, Identification of CodY targets in *Bacillus anthracis* by genome-wide in vitro binding analysis, J. Bacteriol. 195 (2013) 1204–1213, https://doi.org/10.1128/JB.02041-12.
[58] T. Mignot, S. Mesnage, E. Couture-Tosi, M. Mock, A. Fouet, Developmental switch of S-layer protein synthesis in *Bacillus anthracis*, Mol. Microbiol. 43 (2002) 1615–1627, https://doi.org/10.1046/j.1365-2958.2002.02852.x.
[59] T. Ferenci, Trade-off mechanisms shaping the diversity of Bacteria, Trends Microbiol. 24 (2016) 209–223, https://doi.org/10.1016/j.tim.2015.11.009.